Proceedings of the ASME 2010 3rd Joint US-European Fluids Engineering Summer Meeting and 8th International Conference on Nanochannels, Microchannels, and Minichannels
FEDSM-ICNMM2010
August 1-5, 2010, Montreal, Canada

FEDSM-ICNMM2010-31055

VORTEX RING FORMATION IN WALL-BOUNDED DOMAINS

Kelley C. Stewart
Mechanical Engineering, Virginia Tech
Blacksburg, VA, USA

Pavlos P. Vlachos
Mechanical Engineering, Virginia Tech
Blacksburg, VA, USA

ABSTRACT

Vortex ring formation and propagation have been studied extensively in quiescent semi-infinite volumes. However, very little is known about the dynamics of vortex-ring formation in wall-bounded domains where vortex wall interaction will affect both the vortex ring pinch-off and propagation velocity. This study addresses this limitation and studies vortex formation in radially confined domains to analyze the effect of vortex-ring wall interaction on the formation and propagation of the vortex ring.

Vortex rings were produced using a pneumatically driven piston cylinder arrangement and were ejected into a long cylindrical tube parallel to the piston cylinder arrangement which defined the confined downstream domain. Two different domains were studied with diameters twice and four times the size of the piston cylinder. A semi-infinite unbounded volume with no downstream cylinder was also investigated for comparison. The piston stroke-to-diameter ratio (L/D_0) for the studied vortex rings was varied between 0.75 and 3 with corresponding Reynolds numbers, based on circulation, of approximately 500 to 8,000. Velocity field measurements were performed using planar Time Resolved Digital Particle Image Velocimetry (TRDPIV).

The TRDPIV data were processed using an in-house developed cross-correlation PIV algorithm and post processed using Proper Orthogonal Decomposition to remove high frequency noise. The propagation velocity and vorticity were investigated and vortex identification was used to track the changing size, location, and circulation of the vortices. The combination of these parameters was used to investigate the effects of wall interaction on vortex ring formation and propagation.

INTRODUCTION

Vortex rings have been expansively studied with a wide variety of investigation methods and applications, although the majority of vortex ring research involves laminar vortex rings in a semi-infinite volume downstream of an orifice [1-4]. The formation and propagation of vortex rings created using a piston cylinder arrangement has been studied while varying a variety of generator parameters including tube and orifice opening geometries and piston velocity programs [1, 3]. Two models are used to analyze the formation of laminar vortex rings, the slug flow model and the similarity model.

In experimental conditions there exist variations within the orifice exit velocity with respect to time which strays from the slug flow model. The variations within the velocity of the orifice exit can be accounted for by calculating the running mean velocity, $\bar{U}p$ as shown in equation 1, and calculating a velocity program factor as introduced by Glezer [5].

$$\overline{U}_p = \frac{1}{t}\int_0^t u_p dt \qquad 1$$

These two parameters are important to calculate as variations from constant exit velocity in time increase the circulation and momentum of a generated vortex. Program factors for a square wave, ramp wave, and haversine wave were calculated by Diddens as 1, 4/3, and 3/2 respectively [5].

Gharib et al. investigated vortex ring formation using a piston cylinder arrangement. Their work demonstrated a non-dimensional time scale formation number shown in equation 2, where $\bar{U}p$ is the running mean of the piston velocity, t is the duration of piston travel and D_0 is the orifice diameter. Further research has also shown the importance of vortex formation in biological systems for the transport of fluid such as in the left ventricle past the mitral valve [6, 7].

$$\frac{L}{D_0} = \frac{\overline{U}_p t}{D_0} \qquad 2$$

A smaller number of studies have also been performed on turbulent vortex rings. There are two main types of turbulent vortex rings: high Reynolds number vortex rings which are initially turbulent and vortex rings which are initially laminar and transition to turbulence by azimuthal bending instabilities. Maxworthy studied the first type of turbulent vortex rings which had Reynolds numbers between 5000 and 15000 [8]. Glezer and Coles also studied a wide range of this type of turbulent vortex rings using laser-Doppler velocimetry and flow visualization techniques while specifically investigating the similarity properties [9]. Weigand and Gharib studied vortex rings with initial Reynolds number of 7500 which underwent azimuthal bending instabilities and transitioned to turbulent vortex rings. The circulation and propagation velocity of the vortex rings were found to decrease in time corresponding with the shedding of vortical structures from the ring [10].

Vortex ring interactions with bodies and walls have been studied both numerically and experimentally [11]. Vortex ring and wall interactions with the vortex ring moving normal to the wall have been studied by Walker et al. [12] and Orlandi et al. [13]. The authors describe the formation of secondary vortex and tertiary vortical structures at the wall using flow visualization and numerical studies. Lim experimentally studied the interaction of a vortex ring with an inclined wall. This study describes the deformation and stretching of the vortex ring as it approaches the wall and the following helical vortex lines as the vortex ring unevenly impinges the wall. There exists an asymmetric rebound phenomenon and formation of a secondary vortical structure [14]. Chang et al. studied an elliptical vortex ring between two no-slip parallel walls numerically and with flow visualization where counter rotating secondary vortical structures were formed at the wall.

The current study explores the formation and propagation of vortex rings in confined cylindrical domains and compare with vortex rings created in a semi-infinite domain using a piston cylinder arrangement. The vortex ring propagation velocity and circulation strength are examined using time resolved planar particle image velocimetry to determine the affects of downstream confined domains of vortex ring formation and propagation.

NOMENCLATURE

D = diameter of varying outer cylindrical domain
D_0 = Piston cylinder diameter
D_{VR} = Vortex ring diameter
L = Length of piston stroke
L/D_0 = Ratio of piston stroke length to piston cylinder diameter
P = piston velocity program factor
Re_J = Reynolds number incorporating the piston velocity profile
$\bar{U}p$ = running mean piston velocity
U_{piston} = peak piston velocity
T = total time of vortex ring ejection
TRDPIV = Time Resolved Digital Particle Image Velocimetry
t = time
u_p = instantaneous piston velocity
Γ = circulation
Γ_{peak} = peak circulation
Γ_{slug} = circulation calculated using the slug model approximation
ν = kinematic viscosity

METHODS

Experimental Setup

Experimental TRDPIV studies of vortex ring formation in downstream cylindrically confined domains of varying diameters allowed for the first time the investigation of vortex ring formation and propagation with cylindrical wall-bounded domains. Vortex rings were produced using a pneumatically driven piston cylinder and propagated within a long cylindrical tube parallel to the piston cylinder arrangement. This cylindrical wall-bounded region defined the confined downstream domain, as shown in Figure 1. Two different confined cylindrical domains were studied with diameters twice and three times the size of the piston cylinder labeled as D/D_0=2 and D/D_0=3 where D is the diameter of the cylindrical domain and D_0 is the piston cylinder diameter. The cylindrical tubes were made of acrylic and were optically clear. A semi-infinite downstream volume with no downstream cylinder was also investigated for comparison. The piston stroke to diameter ratio (L/D_0) for the studied vortex rings was varied between 0.75 and 3 with corresponding Reynolds numbers of approximately 500 to 8,000. Velocity field measurements were performed using TRDPIV. Figure 1 displays two views of the TRDPIV experimental setup.

Vortex Ring Generation Conditions

Vortex rings were generated by a discharge of fluid from a piston cylinder arrangement driven by a pneumatic cylinder over a finite time interval. The piston cylinder's travel distance was determined based on the designed L/D_0 values. This process can be estimated by considering the slug-flow model where we assume uniform flow over the circular outlet jet and we neglect the initial transient period [1, 4, 15].

The pneumatic cylinder was used in combination with a Teflon piston cap to produce the vortex rings. The piston moved inside a 0.5 inch inner diameter acrylic cylinder and the region of interest began immediately downstream of the small piston cylinder's end. The velocity of the piston cylinder varied in time associated with a specific velocity program. The velocity of the piston cylinder was measured using a Novotechnik linear TLH series potentiometer. The mean velocity with respect to time was calculated using equation 3, where $u_p(t)$ is the velocity of the piston cylinder, which is assumed to be constant over the jet area, at time t and T is the total ejection time interval.

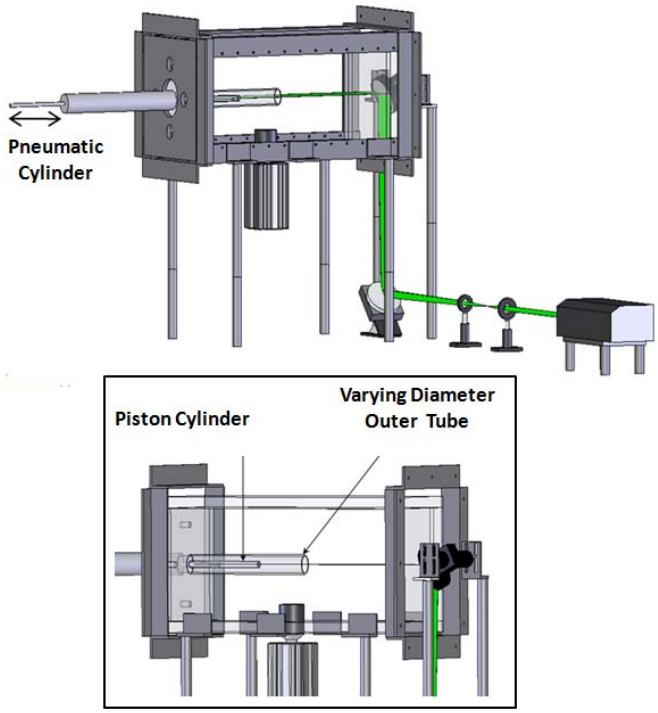

Figure 1: Schematic of vortex ring formation experimental setup with varying downstream diameter conditions.

$$\overline{U_p} = \frac{1}{T}\int_0^T u_p(t)dt \qquad 3$$

Variations within the specific velocity program are adjusted for by introducing a velocity program factor P. This value is calculated in equation 4. The velocity program factor accounts for increases in vortex ring circulation and momentum associated with variations in the velocity program [5].

$$P = \int_0^1 \left(\frac{U_p^2}{\overline{U}_p^2}\right) d\left(\frac{t}{T}\right) = \frac{\overline{U_p^2}}{\overline{U}_p^2} \qquad 4$$

Experimental Testing Conditions

The experimental testing conditions, L/D_0 values, were chosen to produce a range of Reynolds numbers (Γ_{slug}/ν) where circulation, Γ_{slug} is calculated using equation 5. Table 1 displays the experimental test matrix with L/D_0 values ranging from 0.75 to 3 and corresponding Γ_{slug} values ranging from 500 to 8,000. Cases with a D/D_0 value of N/A have no downstream confinement.

$$\Gamma_{slug} = \frac{1}{2} t \overline{U}_p^2 \qquad 5$$

Table 1: Experimental Test Matrix

Case #	Re	L/D_0	D/D_0
1.1	594	0.75	N/A
1.2	1454	1	N/A
1.3	3091	1.5	N/A
1.4	3328	2	N/A
1.5	5663	2.5	N/A
1.6	6893	3	N/A
2.1	517	0.75	3
2.2	1989	1	3
2.3	3200	1.5	3
2.4	4588	2	3
2.5	7524	2.5	3
2.6	8741	3	3
3.1	522	0.75	2
3.2	1100	1	2
3.3	2613	1.5	2
3.4	3900	2	2
3.5	5400	2.5	2
3.6	7530	3	2

TRDPIV Experimental Procedures

Planar TRDPIV is an optical flow measurement technique which uses a coherent light source to illuminate a region of interest. The coherent light source is expanded into a thin plane and directed over a region of interest parallel to a high speed camera lens face. The flow is seeded with neutrally-buoyant flow tracer particles; the movement of these flow tracer particles is captured by high speed images. Cross correlation techniques are used to obtain planes of velocity vectors within the region of interest from the flow tracer displacements between high speed images.

The laser plane was positioned parallel to the piston cylinder, as shown in Figure 1, and the high speed camera was positioned below the test setup perpendicular to the laser plane. All data was acquired using a kHz Nd:YAG dual Head laser. Laser pulses separated by 0.02 – 0.003 seconds according to L/D_0 value were used to acquire data synchronized with an IDT XS-5 CMOS camera. The images acquired within this region were 1280 pixels by 800 pixels. The magnification was optimized at 62 microns per pixel. Neutrally-buoyant polystyrene spheres with 10 μm were used as flow tracers.

Cross correlation algorithms were performed to calculate the velocity fields on a uniform grid of 199x319 locations with a vector grid spacing of 4 pixels or 248μm. Three passes of a robust phase correlation based deformation method algorithm were used with a grid resolution of 16x16 vectors and a window resolution of 32x32 vectors on the first two passes [16-19]. The final pass had a grid resolution of 4x4 and a window resolution of 16x16 vectors. Area validation using median filters on grids of 7x7 vectors were implemented in order to

remove stray vectors. Based on the magnification and the laser timing, a typical displacement of the flow tracers between correlated frames was on the order of 3-6 pixels.

Table 2: Laser Pulse Separation Matrix

L/D_0	Laser Pulse Separation (sec)
0.75	0.0200
1	0.0100
1.5	0.0055
2	0.0045
2.5	0.0045
3	0.0045
4	0.0030
5.5	0.0030
7	0.0030

Proper Orthogonal Decomposition

Proper Orthogonal Decomposition is a technique for decomposing a flow field into its fundamental components. The method calculates the optimal basis functions and determining the energy contained in each of these modes [20, 21]. POD was used to post process the TRDPIV results in order to remove high frequency noise. In this analysis the flow fields were reconstructed with the fundamental eigenmodes which contained 95% of the total energy in the system.

Vortex Identification Scheme

A local vortex identification scheme was used to determine the location of vortex rings using the Δ criterion where the vortex core is defined as the region where the curl of the velocity vector has complex eigenvalues, refer to Chong and Perry and Chakraborty et al. [22, 23]. Using this method, vortex centers were located. The circulation strength of each vortex was calculated using equation 6 around a closed contour determined by a constant Δ criterion function value.

$$\Gamma = \oint_C u \cdot ds \qquad 6$$

Generated Vortex Rings

Vortex rings were generated at 6 Reynolds numbers into a semi-infinite downstream volume. Figure 2 displays the vorticity field and velocity magnitude field for an unconfined vortex ring with $L/D_0 = 2$. The piston velocity factor varied from 1.12 to 1.39. This range of values appropriately corresponds to Glezer's value for a ramp velocity program of 4/3, which is most similar to this study's velocity program. The calculated velocity program is used as a modified Reynolds number shown in equation 7 as defined by Glezer [5].

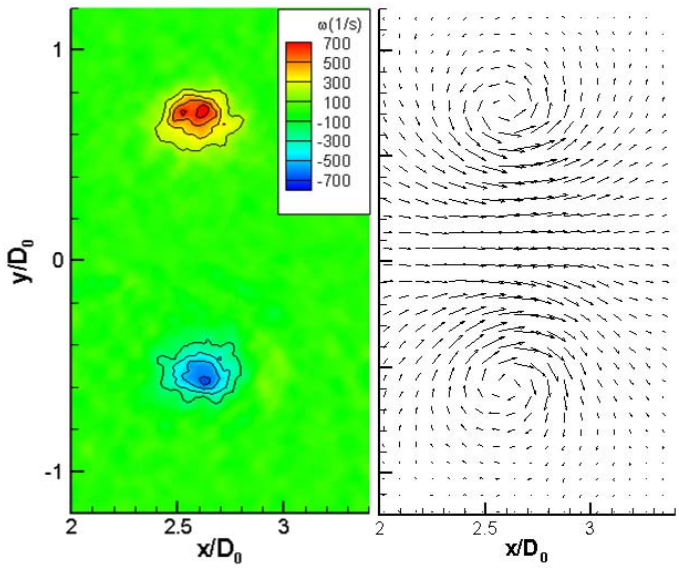

Figure 2: Vorticity (left) and velocity magnitude vectors (right) for an unconfined $L/D_0 = 2$ vortex ring.

$$\mathrm{Re}_J = \frac{P\overline{U}_p L_0}{\nu} \qquad 7$$

The Reynolds Number parameter, Re_J, accounts for the piston velocity profile and provides a non-dimensional parameter for characterizing vortex ring circulation strength. Figure 3 displays the peak circulation divided by kinematic viscosity (Γ_{peak}/ν) versus the Re_J parameter with each square corresponding to a single vortex ring L/D_0 generation condition with no confined downstream domain. The peak circulation used in this analysis was calculated using equation 6 and taking the average circulation strength at the end of the vortex development where circulation strength is at its peak. The plotted solid line represents the best fit trend line from Glezer's analysis of Didden's data where the data collapses onto a single trend line when the velocity profile, P, was incorporated into the denominator Re_J parameter [5]. The current data follows the trend line generated by Glezer using the generating conditions L/D_0=0.75 to L/D_0=2 which are the leftmost four locations. The data analyzed by Glezer to which the trend line was fit only included data with L/D_0 values of 0.6-2.2 which may explain the dissimilarity in the larger L/D_0 values of the present analysis with Re_J values greater than 5,500 shown as a dashed line.

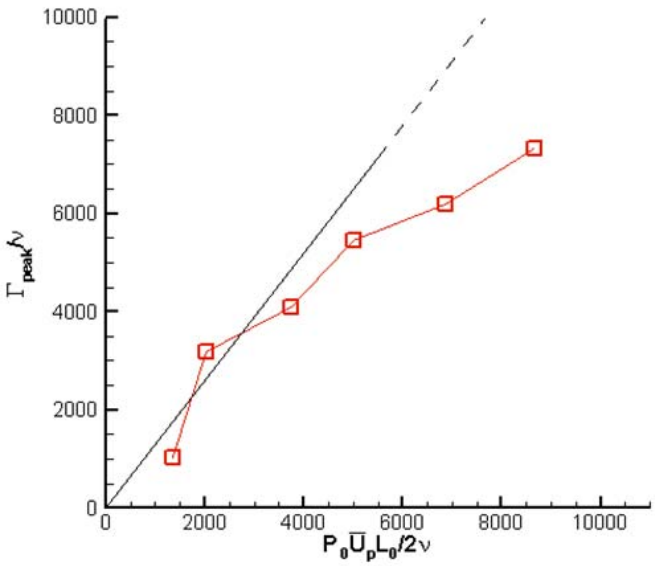

Figure 3: Circulation of generated vortex rings with no downstream confinement

Results

The behavior of the unconfined vortex rings within this experiment is consistent with previously studied vortex rings produced by a piston cylinder arrangement. Vortex rings generated with downstream confined domains were compared to unconfined vortex ring produced in the current as well as previous studies. It was expected that the behavior of the vortex rings produced with confined domains would differ from an unbounded domain, but to what extent these differences exist was previously unexplored.

Figure 4 displays the peak circulation divided by the kinematic viscosity (Γ_{peak}/ν) versus the Re_J parameter, similar to Figure 2. This plot shows that the introduction of the confined cylindrical domain does not drastically affect the relationship of Γ_{peak}/ν and Re_J and does not change the peak circulation strength values. Once again the data points for L/D_0 values < 2.5 follow Glezer's previously reported data trend line well but the data strays from the trend line with L/D_0 values of 2.5 and 3. The higher L/D_0 values may enter a nonlinear regime or do not follow the same trends as the lower laminar L/D_0 values.

Although the initial vortex ring formation was relatively uninfluenced by the addition of confined downstream boundaries, the velocity and circulation strength as the vortex ring propagates was greatly affected. The propagation velocity of the vortex rings, shown in Figure 5, displays the propagation velocity of the vortex ring before departing from the region of interest or beginning vortex ring dissipation in the case of the confined vortex rings. The propagation velocities are normalized by the peak piston velocity U_{piston} and are plotted versus Re_J. The red squares correspond to the no outer cylinder case and match well with the formula for the speed of a thin cored vortex [24]. The vortex rings generated with confined downstream domains show progressively lessened propagation velocities as the confined domain diameter decreases.

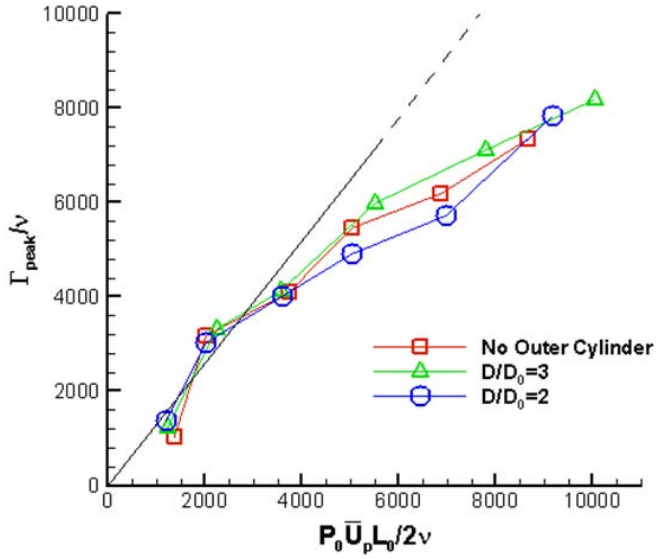

Figure 4: Circulation of generated vortex rings with varying downstream domain conditions

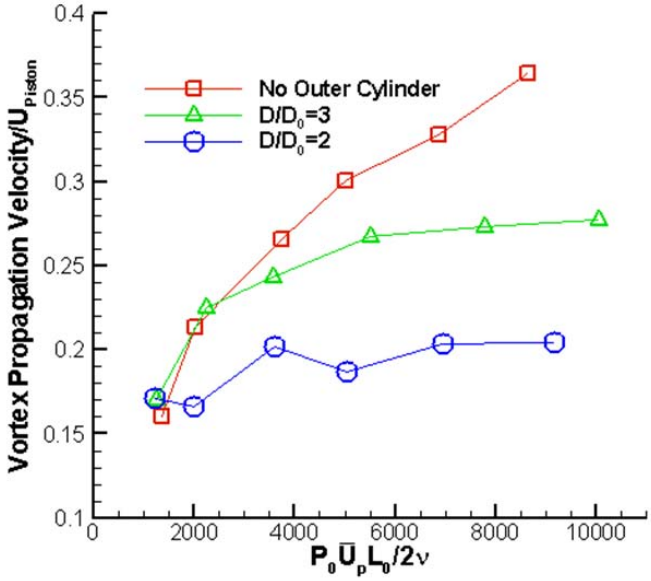

Figure 5: Propagation velocity of generated vortex rings with varying downstream domain conditions

The positive circulation strengths for each generated vortex ring are plotted with respect to the non-dimensional formation time, introduced in equation 2, in Figure 6, Figure 7, and Figure 8 with no outer cylinder, D/D_0=3 and D/D_0=2 respectively. In Figure 6, the no outer cylinder case, the

positive circulation strength increases as the formation time increases until it reaches a plateau and the circulation strength remains constant. The formation time when the positive circulation strength levels off corresponds to the L/D_0 value of the vortex ring. Figure 7 displays the normalized circulation strength versus the formation time for the D/D_0 =3 case. The positive circulation patterns are very similar to the no outer cylinder cases except the circulation strength values display a slight decay over time.

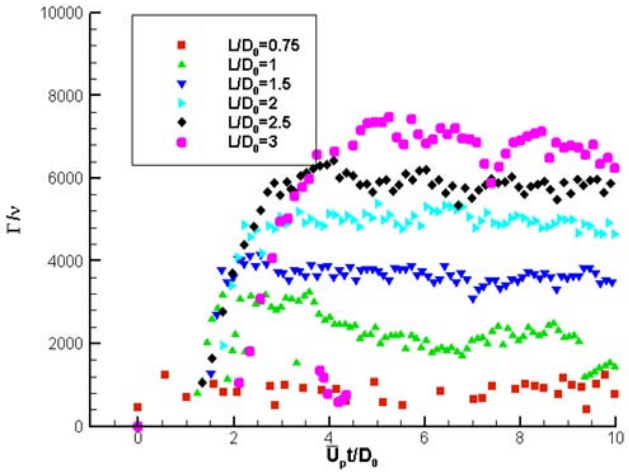

Figure 6: Circulation strength versus formation time for vortex rings generated with no outer cylinder domain.

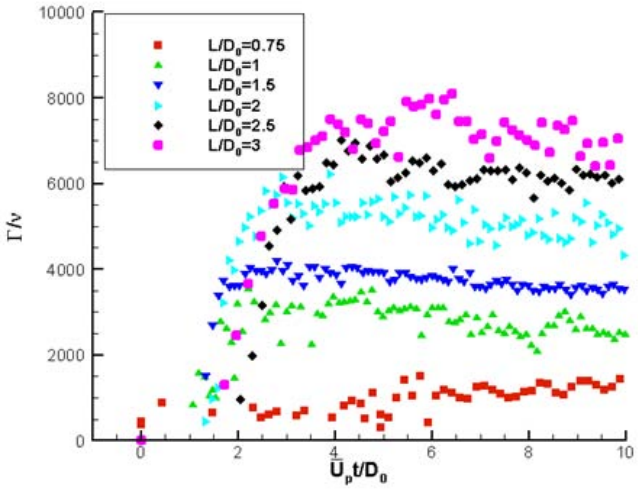

Figure 7: Circulation strength versus formation time for vortex rings generated with the outer cylinder domain D/D_0 = 3.

Figure 8 displays the normalized circulation strength versus formation time for the D/D_0=2 cases. The circulation strength lines for each L/D_0 case show a drastically different pattern than the D/D_0=3 cases and the no outer domain cases. The initial formation and growth region of each L/D_0 case remains relatively unaltered, but there is no circulation strength plateau region. The Γ/ν values begin to decline at a similar rate of decay for all L/D_0 values.

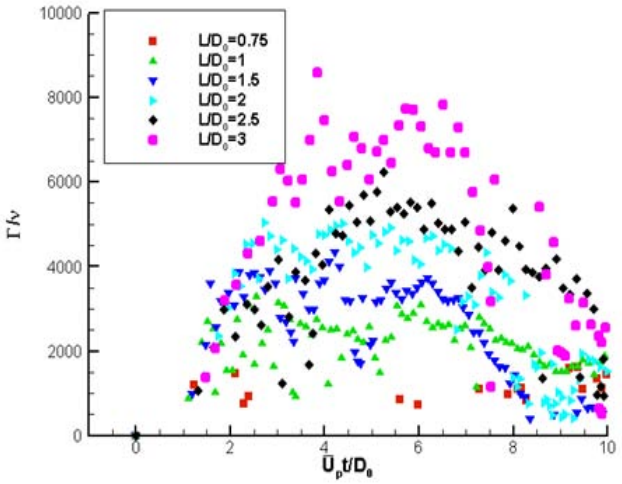

Figure 8: Circulation strength versus formation time for vortex rings generated with the outer cylinder domain D/D_0 = 2

Figure 9 displays three time instances for the L/D_0=2 case for the three downstream domains. For the no outer diameter case and the D/D_0=3 case the vortex ring is formed and smoothly propagates along the X/D_0 axis. The D/D_0=3 case shows a larger decline in the velocity magnitude in the t=0.290 seconds frame than the no outer cylinder case which is consistent with the circulation strength results shown in Figure 6 and Figure 7. The D/D_0=2 case shows a slug velocity along the entire diameter of the tube in the t=0.146 seconds frame which is dissipated before the t=0.234 seconds frame. This velocity can also faintly be seen in the D/D_0=3 t=0.146 seconds frame. The smallest outer cylinder case shows a normal vortex ring with a slightly reduced propagation velocity in the t=0.234 seconds frame but shows the vortex ring at reduced X/D_0 position and tilted from vertical in the t=0.290 seconds case. This represents the beginning of the dissipation and decay of the D/D_0=2 vortex ring.

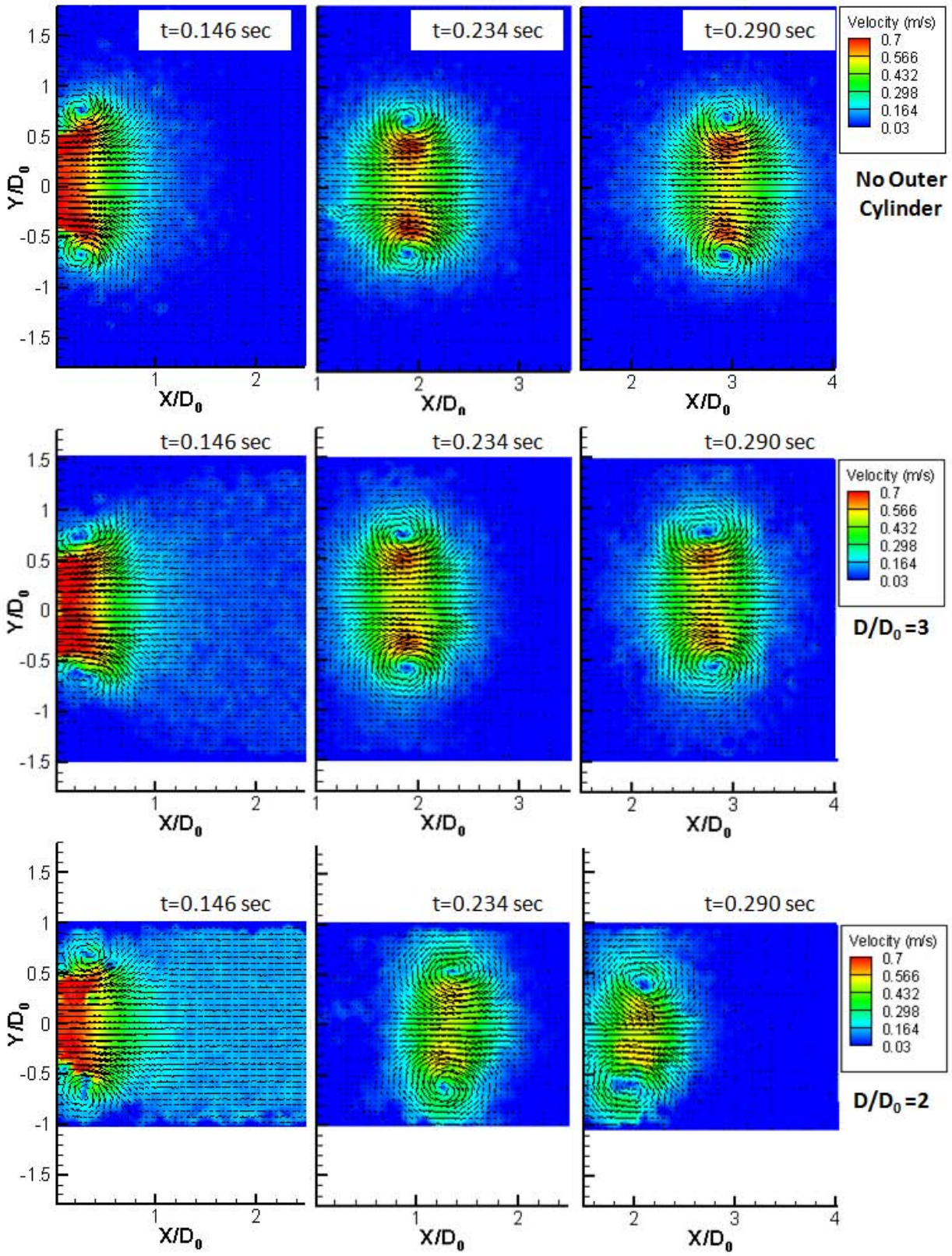

Figure 9: $L/D_0=2$ vortex ring formed with no outer cylinder domain (top), $D/D_0=3$ domain (center), and $D/D_0=2$ domain (bottom). The walls and outside region are masked in the $D/D_0=3$ and $D/D_0=2$ cases.

DISCUSSION AND CONCLUSIONS

The dynamics of vortex rings produced with a piston cylinder with varying downstream domains are investigated to determine the affect of confined downstream domains on vortex ring formation and propagation. Figure 4 displays the formation and peak circulation strength of the generated vortex ring are relatively unaltered by the confined downstream domain. The propagation velocity of the generated vortex rings was greatly decreased by the presence of a confined downstream domain. The $D/D_0=2$ case shows very little increase in normalized propagation velocity with increasing Re_J value. The circulation strength normalized by viscosity for the $D/D_0=2$ cases also show drastically different dynamics than the unconfined domain case. The vortex ring formation is minimally affected but after the formation process, the vortex ring immediately begins to dissipate leading to the decay of circulation strength in Figure 8.

It is assumed that the decay of the confined vortex in the $D/D_0=2$ case is initiated by the formation of a secondary counter rotating vortex along the cylindrical confinement wall which causes the primary vortex to begin to stray from its horizontal orientation. The primary vortex begins to tumble over its axis and break down the vortex ring structure as it dissipates. Further investigation and analysis is necessary to continue to investigate the affects of confined downstream domains on the formation and propagation of piston cylinder generated vortex rings.

REFERENCES

[1] Krueger, P., 2008, "Circulation and trajectories of vortex rings formed from tube and orifice openings," Physica D: Nonlinear Phenomena, 237(14-17), pp. 2218-2222.

[2] Weigand, A., and Gharib, M., 1997, "On the evolution of laminar vortex rings," Experiments in Fluids, 22(6), pp. 447-457.

[3] Pullin, D., 1979, "Vortex ring formation at tube and orifice openings," Physics of Fluids, 22, p. 401.

[4] Didden, N., 1979, "On the formation of vortex rings: rolling-up and production of circulation," Zeitschrift für Angewandte Mathematik und Physik (ZAMP), 30(1), pp. 101-116.

[5] Glezer, A., 1988, "The formation of vortex rings," Physics of Fluids, 31, p. 3532.

[6] Dabiri, J. O., 2009, "Optimal Vortex Formation as a Unifying Principle in Biological Propulsion," Annual Review of Fluid Mechanics, 41, pp. 17-33.

[7] Dabiri, J. O., and Gharib, M., 2005, "The role of optimal vortex formation in biological fluid transport," Proceedings of the Royal Society B-Biological Sciences, 272(1572), pp. 1557-1560.

[8] Maxworthy, T., 1974, "Turbulent vortex rings," Journal of Fluid Mechanics, 64(02), pp. 227-240.

[9] Glezer, A., and Coles, D., 1990, "An experimental study of a turbulent vortex ring," Journal of Fluid Mechanics, 211, pp. 243-283.

[10] Weigand, A., and Gharib, M., 1994, "On the decay of a turbulent vortex ring," Physics of Fluids, 6, p. 3806.

[11] Rockwell, D., 1998, "Vortex-body interactions," Annual Review of Fluid Mechanics, 30(1), pp. 199-229.

[12] Walker, J. D. A., Smith, C. R., Cerra, A. W., and Doligalski, T. L., 1987, "THE IMPACT OF A VORTEX RING ON A WALL," Journal of Fluid Mechanics, 181, pp. 99-140.

[13] Orlandi, P., and Verzicco, R., 2006, "Vortex rings impinging on walls: axisymmetric and three-dimensional simulations," Journal of Fluid Mechanics, 256, pp. 615-646.

[14] Lim, T., 1989, "An experimental study of a vortex ring interacting with an inclined wall," Experiments in Fluids, 7(7), pp. 453-463.

[15] Shariff, K., and Leonard, A., 1992, "VORTEX RINGS," Annual Review of Fluid Mechanics, 24, pp. U235-U279.

[16] Eckstein, A., and Vlachos, P., 2009, "Digital particle image velocimetry (DPIV) robust phase correlation," Measurement Science and Technology, 20, p. 055401.

[17] Eckstein, A., and Vlachos, P., "A robust phase correlation DPIV processing algorithm for time resolved measurements."

[18] Scarano, F., 2002, "Iterative image deformation methods in PIV," Measurement Science and Technology, 13, pp. R1-R19.

[19] Eckstein, A., and Vlachos, P., 2009, "Assessment of advanced windowing techniques for DPIV," Measurement Science and Technology, 20, p. 075402.

[20] Sirovich, L., 1987, "Turbulence and the dynamics of coherent structures. I- Coherent structures. II- Symmetries and transformations. III- Dynamics and scaling," Quarterly of applied mathematics, 45, pp. 561-571.

[21] Doligalski, T., Smith, C., and Walker, J., 1994, "Vortex interactions with walls," Annual Review of Fluid Mechanics, 26(1), pp. 573-616.

[22] Chong, M., Perry, A., and Cantwell, B., "A general classification of three-dimensional flow fields," Cambridge Univ Pr, p. 408.

[23] Chakraborty, P., Balachandar, S., and Adrian, R., 2005, "On the relationships between local vortex identification schemes," Journal of Fluid Mechanics, 535, pp. 189-214.

[24] Saffman, P., 1995, Vortex dynamics, Cambridge Univ Pr.